

The Large-Grained Dust Coma of 174P/Echeclus

JAMES M. BAUER, YOUNG-JUN CHOI,¹ AND PAUL R. WEISSMAN
Jet Propulsion Laboratory, California Institute of Technology, MS 183-501, Pasadena, CA

JOHN A. STANSBERRY
Steward Observatory, University of Arizona, Tucson AZ

YANGA R. FERNÁNDEZ
Department of Physics, University of Central Florida, Orlando, FL

HENRY G. ROE
Lowell Observatory, Flagstaff, AZ

BONNIE J. BURATTI
Jet Propulsion Laboratory, California Institute of Technology, MS183-501, Pasadena, CA

AND
HYUN-IL SUNG
Korea Astronomy and Space Science Institute, 61-1 Hwaam-dong, Yuseong-gu, Daejeon 305-348 South Korea

Received 2007 September 18; accepted 2008 February 15; published 2008 April 11

ABSTRACT. On 2005 December 30, Y.-J. Choi and P. R. Weissman discovered that the formerly dormant Centaur 2000 EC98 was in strong outburst. Previous observations by P. Rousselot et al. spanning a 3-year period indicated a lack of coma down to the 27 mag arcsec⁻² level. We present *Spitzer Space Telescope* MIPS observations of this newly active Centaur—now known as 174P/Echeclus (2000 EC98)—or 60558 Echeclus—taken in 2006 late February. The images show strong signal at both the 24 and 70 μm bands and reveal an extended coma about 2' in diameter. Analyses yield estimates of the coma signal contribution that are in excess of 90% of the total signal in the 24 μm band. Dust production estimates ranging from $1.7\text{--}4 \times 10^2 \text{ kg s}^{-1}$ are on the order of 30 times that seen in other Centaurs. Simultaneous visible-wavelength observations were also obtained with Palomar Observatory's 200-inch telescope, the 1.8-m Vatican Advanced Technology Telescope, the Bohyunsan Optical Astronomy Observatory (BOAO) 1.8-m telescope, and Table Mountain Observatory's 0.6-m telescope, revealing a coma morphology nearly identical to the mid-IR observations. The grain size distribution derived from the data yields a log particle mass power-law with slope parameter $\alpha = -0.87 \pm 0.07$, and is consistent with steady cometary activity, such as that observed during the *Stardust* spacecraft's encounter at 81P/Wild 2, and not with an impact-driven event, such as that caused by the Deep Impact experiment.

1. INTRODUCTION

Centaurs are icy bodies orbiting among the giant planets of the Solar System that have recently (within a few million years; Horner et al. 2004) escaped from the scattered disk of the Kuiper Belt. As such, they are considered transition objects between the inactive trans-Neptunian objects and short-period inner Solar System comets. About 10%–15% of the known Centaurs are accepted as having had observed cometary activity,

usually episodically, in bursts. However, the start of a major outburst on a Centaur had rarely been witnessed. Choi et al. (2006b) reported observations of a formerly inactive Centaur, 2000 EC₉₈ (now 174P/Echeclus; Choi et al. 2006a) that indicated the presence of a strong coma. The coma persisted through the end of 2006 July, while the apparent distance between the primary and the coma's brightness center steadily grew (Choi & Weissman 2006; Choi et al. 2006a). Previously observations of (60558) Echeclus at visible through IR wavelengths indicated an apparently inactive surface, unobscured by coma (Delsanti et al. 2006; Rousselot et al. 2005; Stansberry et al. 2005; Bauer et al. 2003a). However, subsequent analyses of

¹ Current address: Korea Astronomy and Space Science Institute, 61-1 Hwaam-dong, Yuseong-gu, Daejeon 305-348, South Korea.

archival data suggest the presence of very faint coma at discrete times (Choi et al. 2006a). We requested *Spitzer Space Telescope* (*Spitzer*) director's discretionary time to observe 174P/Echeclus using the Multi-band Imaging Photometer (MIPS) at 24 and 70 μm . At the time of proposal submission, we had no way of knowing whether the Centaur would still be active by the time the observations occurred. If inactive, our goals were to observe a surface altered by the recent strong outbursting and compare that with previous observations by *Spitzer*. If active, our goals were to characterize the coma's dust and, if possible, image the nucleus through the coma. In fact, the Centaur was active during our observations, and so we desired to see how quickly and profoundly Centaur surfaces could be altered by activity, and characterize the onset, persistence, and amount of activity.

The differences in active Centaurs are broad. Some exhibit strikingly red colors (Bauer et al. 2003b; Stansberry et al. 2004), while others have neutral to blue comae (Meech et al. 1990). The level of activity varies as well, with dust production rates ranging from a few to several tens of kg s^{-1} (Stansberry et al. 2004). Table 1 summarizes some of these parameters, along with some recently observed shorter period comets, for comparison with 174P/Echeclus (to avoid semantic complications, hereafter Echeclus).

From the time of discovery of its 2005–2006 outburst, the coma of Echeclus has been uniquely intense, by far the most seen from a Centaur, even the very active Schwassmann-Wachmann 1 (Table 1). The mechanism driving the excessive activity is not clear. At the observed distance near 13 AU, the Centaur is too distant for the outburst to be driven by the sublimation of water ice, as is common of comets when they are closer to the Sun (Meech and Svøren, 2004). Other species, such as CO, have been suggested as driving the activity observed in other Centaurs (cf. Meech et al. 1997; Womak and Stern 1995; and Senay & Jewitt 1994). CO ejection mechanisms involving

the amorphous-to-crystalline water-ice transition have also been suggested by Prialnik et al. (1995), Choi et al. (2002), and Jewitt (2007) and are consistent with the onset of activity near 13 AU. The timing of the outburst also differs from other active Centaurs in that for an interval of 5 years, from the time of Echeclus' discovery, no sign of activity had been seen. Pre-outburst limits on coma down to 27 mag arcsec $^{-2}$, or on the order of 4 50 g s^{-1} dust production, were set by Rousselot et al. (2005) and Lorin & Rousselot (2007). Extremes of cometary outburst behavior are not unheard of in comets, as was recently observed in comet 17P/Holmes (Buzzi et al. 2007), and Echeclus' onset of activity did match the heliocentric distance of onset of peak activity for Chiron (cf. Bauer et al. 2004). However, the frequency of the outbursts observed for Centaurs with similar orbits is more regular (Meech et al. 1997; Bauer et al. 2003b), and so it may be that the mechanism for driving activity is unique for Echeclus, as compared with other Centaurs. Our observations were intended in part to explore the possibility of an impact-driven outburst, and to examine how the coma particle size distribution compared to that observed in other cometary bodies.

The outburst of Echeclus also had interesting morphological features. There appears to be an offset in the central condensation of the coma from the location of the nucleus, that varies with time. This offset appeared to at first grow, moving westward to a maximum offset of $\sim 8''$, then lessen and move to the opposite sky-plane side of the nucleus. The MIPS observations were acquired while the westward separation was growing, and was approximately $6''$.

This paper will address primarily the MIPS exposures taken in 2006 and the ground-based imaging taken near the time of these *Spitzer* observations. The outburst discovery observations and the ground-based observations taken over the 2007 season are to be addressed in a paper in preparation by Choi and colleagues, and the dynamical analysis is to be presented in a companion paper in preparation by Weissman and colleagues.

TABLE 1
COMPARISON OF ECHECLUS AND SELECT COMETARY BODIES

Object	$\log(Af\rho)$ (cm)	Q_{dust} (kg s^{-1})	$V - R$	References
<i>Centaurs</i>				
174P/Echeclus	4.0	$\sim 3 \times 10^2$	0.47	This work
166P/NEAT	2.5	~ 1	0.9	Bauer et al. 2003b
60P/Chiron	~ 3.8	$\sim 3\text{--}20$	0.36	Meech & Belton 1990, Fulle 1994
P/2004 A1 (LONEOS)	2.5	~ 1.5	...	Mazzota Epifani et al. 2006
<i>Jupiter Family Comets (JFCs)</i>				
29P/Schwassmann-Wachmann 1 (some-times listed as Centaur)	4.2	30–60	0.55	Szabo et al. 2002, Fulle 1992, Bauer et al. 2003a, Stansberry et al. 2005
9P/Tempel 1	~ 2.4	6–16 ^a	0.4	Bauer et al. 2007
81P/Wild 2	~ 2.4	10–20	0.46	Farnham 2003, Schulz & Stüwe 2000
<i>Typical JFC</i>	2	$\sim 0.2\text{--}0.4$...	A'Hearn et al. 1995

NOTES. Each value is as derived from the listed reference. Where Q_{dust} is not provided, Q_{dust} is derived using the method outlined in Bauer et al. 2003b, assuming a grain size of 1 μm , and $\rho \approx 1.0 \text{ g/cm}^3$.^aThe Q_{dust} value is for the ambient coma before impact, and a range of dust-grain ejection velocities, $v_{\text{ej}} \sim 200\text{--}600 \text{ m s}^{-1}$.

Much of our analysis of our MIPS observations is in reference to pre-outburst observations taken in 2004. The results of the 2004 data are presented by Stansberry et al. (2007).

2. OBSERVATIONS

2.1 Simultaneous Optical Imaging

Images were obtained in *B*, *V*, *R*, and *I* bands at the Jet Propulsion Laboratory’s Table Mountain Observatory (TMO) 0.6-m telescope throughout the night of 2006 February 24 and in *R* band for the nights of 2006 February 4, 9, and 25 (UT). For the nights of February 4 and 9, 300 s integration times were used, with three exposures on February 4 and six exposures on February 9. A total of 19 exposures of duration 900 s were obtained on February 24, and 21 900 s integrations on February 25 were obtained at TMO. We used the facility’s TEK 1024 CCD camera, which has a pixel scale of $0.52''$ and is equipped with a Bessel-type filter set (Bessel, 1990). Single *V*- and *R*-band 600 s exposures were taken at the Bohyunsan Optical Astronomy Observatory (BOAO) 1.8-m telescope on the night of February 24 near 17UT. BOAO is a facility run by the Korea Astronomy and Space Science Institute located in South Korea. The facility camera uses a SITE 2 K back-illuminated CCD chip with read noise 7.0 and detector gain $1.8 e^-/ADU$. The night was clear with median seeing of $2.5''$, and the image pixel scale was $0.34''$. Images were also obtained in *RI* band from the Palomar 200-inch on February 25–27 utilizing the LFC camera, a 6-chip mosaic CCD camera with a 2×2 binned pixel scale of $0.36''$, with a 2048×1024 pixel dimension (for each CCD chip) in the binned mode. The highest quality chip (chip 0) was used to image the Centaur in all the exposures, and the long axis was oriented East to West during the exposures. We obtained a total of three 120 s integrations on the nights of February 25 and 27, and two 120 s exposures on February 26 with the 200-inch. Four images were also obtained at the Vatican Advanced Technology Telescope (VATT), on Mt. Graham in Arizona, using the facility 2 K CCD camera on the night of February 25. Each image was exposed for a total of 500 s through the facility *R*-band filter, which had similar transmission characteristics as the TMO *R*-band filter. The camera’s pixel scale was $0.37''$, and the aver-

age seeing was $1.4''$ over the 4 VATT exposures spanning 8:59–9:38 UT.

The combined data sets give an immediate sense of the visual behavior at the time of the *Spitzer* observations, and provide a larger temporal context for the interpretation of the observed level of activity. A summary of the observing conditions, including the comet’s heliocentric (*R*) and observer (Δ) distances, the viewing phase angle (α), the solar radius vector position angle and projected anti-heliocentric velocity vector ($PA_{\uparrow,R}$), the seeing and photometric conditions, and the approximate angular distance of the coma central condensation from the interpreted nucleus position is provided in Table 2. Over the 4 nights of observations near the *Spitzer* exposures, the average separation was $6.2(\pm 1.3)''$, or a projected distance of $55000(\pm 12000)$ km. The angular separation is determined from the local peak centroid from a sampling size on the order of the seeing; Figure 1 shows the combined images, which reveal the amount of separation around the time of the *Spitzer* observations. A color composite image, generated from *V*-, *R*-, and *I*-band exposures from our February 24 TMO data set, is shown in Figure 2.

February 24 was the only TMO data set taken under photometric conditions, so we conducted relative photometry on the Echeclus imaging data for the nights that were not photometric. Five or more field reference standards were calibrated for each frame. The fields from February 4 and 9 were photometrically calibrated on the night of February 24, as was the field for the night of February 25. None of the Palomar, BOAO, or VATT images were photometrically calibrated during the nights of observation, but the February 25–27 contained forward-calibrated field standards present in the TMO data.

2.2 *Spitzer* MIPS Observations

Spitzer observations were obtained at 11:25 UT on 2006 February 24 and 10:40 UT on 2006 February 25 ($R = 12.97$ AU, $\Delta = 12.48$ AU, and phase $\alpha = 3.97^\circ$). The MIPS 24 and $70 \mu\text{m}$ modes were used in standard photometry mode, with two cycles of 10 s (with 14 dither points) at the shorter wavelength and 20 cycles of 10 s (with 10 dither points) at the longer for total per-pixel exposures of 312.5 and 2180 s, respectively. Shadow observations were made in order to remove background Galactic and extragalactic sources from Echeclus’ coma signal.

TABLE 2
VISUAL BAND OBSERVING CONDITIONS

UT Date/ Telescope	<i>R</i> (AU)	Δ (AU)	α ($^\circ$)	$PA_{\uparrow,R}$ ($^\circ$)	Seeing (arcsec)	Cloud coverage	Coma peak separation (arcsec)
Feb 04/TMO	13.01	12.56	3.95	291, 288	2.1	cirrus	$\leq 6.8(3.3 \pm 3.5)^a$
Feb 09/TMO	13.00	12.48	3.78	291, 288	1.8	thick cirrus	$\leq 5.8(3.3 \pm 2.5)^a$
Feb 24/TMO and BOAO	12.97	12.25	3.0	290, 288	1.9 & 2.4	photometric	$\sim 5.6 \pm 2.7$
Feb 25/TMO, Palomar, and VATT	12.97	12.23	3.0	290, 288	2.0	cirrus at TMO & Palomar; clear at VATT	$\sim 6.6 \pm 2.8$
Feb 26/Palomar	12.97	12.22	2.95	290, 288	1.8	cirrus	$\sim 6.7 \pm 2.5$
Feb 27/Palomar	12.97	12.21	2.90	290, 288	1.5	cirrus	$\sim 6.0 \pm 2.1$

^a The measured separation values are listed in parentheses, but are $< 2\times$ the uncertainty.

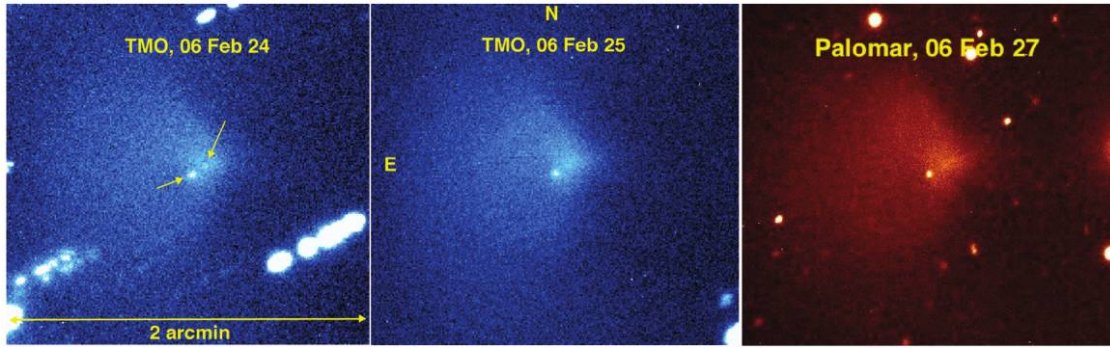


FIG. 1.—*R*-band image from TMO's 0.6-m telescope taken simultaneously with the *Spitzer* MIPS observations (*left and center panels*), and an *RI*-band image (*right panel*) from the Palomar 200-inch telescope taken 2 nights after the observations (similar scales and orientations). Ten 900s TMO exposures were stacked to make each of the images in the left and center panels, and three 120 s Palomar images were stacked to obtain the rightmost image. The data show a $\sim 6''$ separation between the coma central condensation (*right arrow, left image*) and 2000 EC98's nucleus (*left arrow, left image*). The Palomar image reveals that the coma structure was stable over several days.

We scheduled the shadow observations *before* the primary exposures in order to avoid contamination of the background field by the dust trail a cometary coma may leave behind. The shadow observations also contained Echeclus at both wavelengths, although a portion of the comet fell outside the $70\ \mu\text{m}$ image's field of view (FOV). The $24\ \mu\text{m}$ exposures covered a total $7.5 \times 8.2'$ FOV with the longer axis oriented 20° East of North, and with the central $3.2 \times 3'$ FOV illuminated during the total integration time and throughout the dither pattern. The $70\ \mu\text{m}$ image had a total FOV of $3 \times 7.9'$ with the long axis oriented 24° East of North, and the central $2.3 \times 2.7'$ illuminated for the total



FIG. 2.—*VRI*-band color composite image from TMO's 0.6-m telescope taken simultaneously with the *Spitzer* MIPS observations on 2006 February 24. The image was made by combining 3 *V*-, 3 *I*- and 5 *R*-band 900 s exposures. The coma is redder than neutral in color ($V - R = 0.50 \pm 0.02$, where solar $V - R = 0.36$).

integration time. The pixel scale at 24 and $70\ \mu\text{m}$ was $2.45''$ and $4''$, respectively. At $24\ \mu\text{m}$, *Spitzer*'s resolution was $6''$, so we were able to barely resolve separate coma and nucleus peaks (Fig. 3). Resolving the separate peaks was not possible at $70\ \mu\text{m}$ with its resolution of $18''$. On the nights of the observations, the $6''$ separation between Echeclus and the coma brightness peak corresponded to $\sim 55,000$ km projected distance on the plane of the sky, consistent with the visible-wavelength observations.

3. REDUCTION AND ANALYSIS

3.1 Visual-Band Imaging

The data reduction for the visual-band images taken at TMO, BOAO, the VATT, and Palomar were similar in most respects, utilizing the standard image processing routines in IRAF (Tody et al. 1986). Individual exposures were bias and flat-field cor-

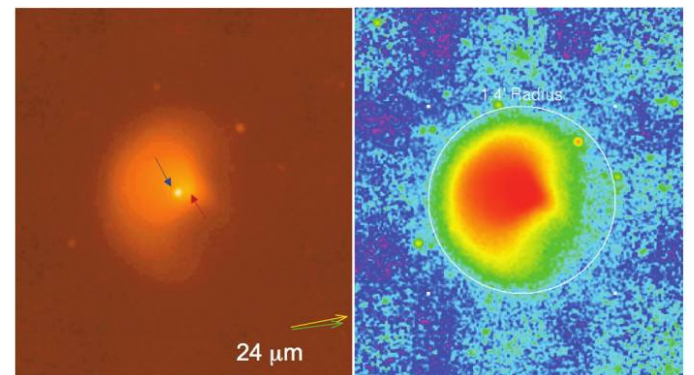


FIG. 3.—February 24 $24\ \mu\text{m}$ *Spitzer* image at $6''$ resolution, in low-contrast (*left*) and false-color high contrast (*right*). In the left panel, the central condensation of the coma (*red arrow*) is barely resolved apart from the Centaur (*blue arrow*), while the Sun-Comet sky-plane vector (*yellow arrow*) is offset only $\sim 3^\circ$ from the sky-plane motion (*green arrow*). The upper bound on the extent of the coma is demarcated by the white circle in the right panel.

TABLE 3
ECHECLUS' COLORS ON THE NIGHT OF 2006 FEBRUARY 24

Aperture Radius (arcsec)	m_R	$B - V$	$V - R$	$R - I$
TMO				
5	18.09 ± 0.02^a	0.72 ± 0.03	0.55 ± 0.03	0.52 ± 0.02
10	16.84 ± 0.02	0.78 ± 0.03	0.47 ± 0.03	0.48 ± 0.03
30	15.18 ± 0.04	0.81 ± 0.07	0.50 ± 0.06	0.58 ± 0.05
Average of 5" to 30" aperture values	0.77 ± 0.06	0.51 ± 0.04	0.52 ± 0.04
BOAO				
5	18.10 ± 0.03^a	...	0.53 ± 0.05	...
10	16.83 ± 0.02	...	0.49 ± 0.05	...
30	15.09 ± 0.02	...	0.51 ± 0.05	...
Combined Annular colors				
5"-10" Annulus	17.25 ± 0.06	0.81 ± 0.09	0.46 ± 0.06^b	0.46 ± 0.08
10"-30" Annulus	15.44 ± 0.07	0.82 ± 0.10	0.51 ± 0.06^b	0.62 ± 0.09

^aThe color and magnitude uncertainties are from photon statistics and sky background level, except the fourth row's average, where the standard deviation is shown as the error.

^bIncludes both TMO and BOAO color data.

rected, and standard star fields (Landolt 1992) were obtained at TMO during our single photometric night on February 24. Field standards from prior and future nights were calibrated on the night of February 24, so that relative photometry could be performed across the data sets. The images taken in the same filters for each night were co-registered and co-added. Background stars in the proximity of Echeclus were removed from the individual exposures before combining the images, as were cosmic rays. Two images were created for each set of exposures, one with images shifted at the comet's predicted rate of motion according to the Horizons ephemeris,² and one with the stars co-aligned for PSF comparison in the analysis. R -band composite images taken February 24 and 25 from TMO and on February 27 from the Palomar 200-inch are shown in Figure 1. The appearance of the comet in all three images is nearly identical.

A color composite made from averages of 3 V , 5 R and 3 I -band exposures is shown in Figure 2. The coma shows a nearly neutral color, and is not very different from that of the nucleus of Echeclus in the image. Color photometry was completed for the night of February 24 using the Bessel B -, V -, R -, and I -band images (Bessel 1990). We sampled the signal at different apertures centered on the nucleus to detect changes in color over the coma's extent (Table 3). Except for slightly larger $V - R$ and $R - I$ color values and smaller $B - V$ colors near the nucleus, we detected no significant differences for apertures greater than 10" in radius. The color values for annuli at 5"-10" and 10"-30" radii, with the central signal subtracted, are also included in Table 3. The only significant difference in the colors between annuli with increasing distance is in the $R - I$ value, though

only within 2 σ of the formally propagated photometric uncertainties. The BOAO data, also included in Table 3, confirm our V - and R -band magnitudes and $V - R$ colors we found in the TMO data. $Af\rho$ values (in $\log_{10}[\text{cm}]$ units) derived from the TMO February 24 observations for the 30" aperture radius in each of the filters are also listed in Table 4, with formal uncertainty owing to photon noise, along with the R -band value from February 25 for comparison. The highest $Af\rho$ values occur in the I band, and are $\sim 25\%$ larger than the R -band values, and a trend of larger $Af\rho$ values at longer wavelengths across all four filters exists. If one uses these values as a proxy for dust, there is an implication of a trend toward redder dust particles. The work of Kolokolova (2001) indicates that dust-grain colors are dictated more by grain size than by albedo variations. The implications here are that larger-grained particles dominate the coma. The images taken on the night of the February 24 have the least background objects, and the total magnitude within a 120" photometry aperture radius yields a value of 14.36 ± 0.02 . Assuming previously measured nucleus brightness values, the coma comprised about 98% of the total visual-band signal during the *Spitzer* observations.

Surface-brightness profiles (SBPs) were produced from the R -band images taken over each night, using the methods described previously in the literature (Meech et al. 1997; Bauer et al. 2003a, 2003b). The profile from February 09 and February 25, 2006 are shown in Figure 4. As mentioned previously one set of co-added images were combined and shifted to match the comet's motion on the sky while another co-added image was generated so that the background stars were aligned. The SBPs for the comet shifted images are shown as individual points with associated error bars, which represent the 1 - σ uncertainty based on photon statistics and calibration uncertainty. Between three and five comparison stellar PSFs were sampled and aver-

²For more information, see the NASA JPL Solar System Dynamics Web site at <http://ssd.jpl.nasa.gov>.

TABLE 4
ECHECLUS' $Af\rho$ VALUES FOR 30" APERTURE RADIUS

Aperture Radius (")	$\log(Af\rho)$
<i>B</i> -band	3.89 ± 0.01
<i>V</i> -band	3.96 ± 0.01
<i>R</i> -band	4.01 ± 0.01
<i>I</i> -band	4.11 ± 0.01
2006 Feb 25, <i>R</i> -band	4.04 ± 0.01

aged from the star-aligned co-added image; the average stellar SBP is shown in red.

The data over the dates spanning the *Spitzer* observations, February 24–27, showed no variation in the *R*-band magnitudes (Table 5) or the SBPs, and even the SBP from over two weeks prior shows little detectable difference (Fig. 4). This steady be-

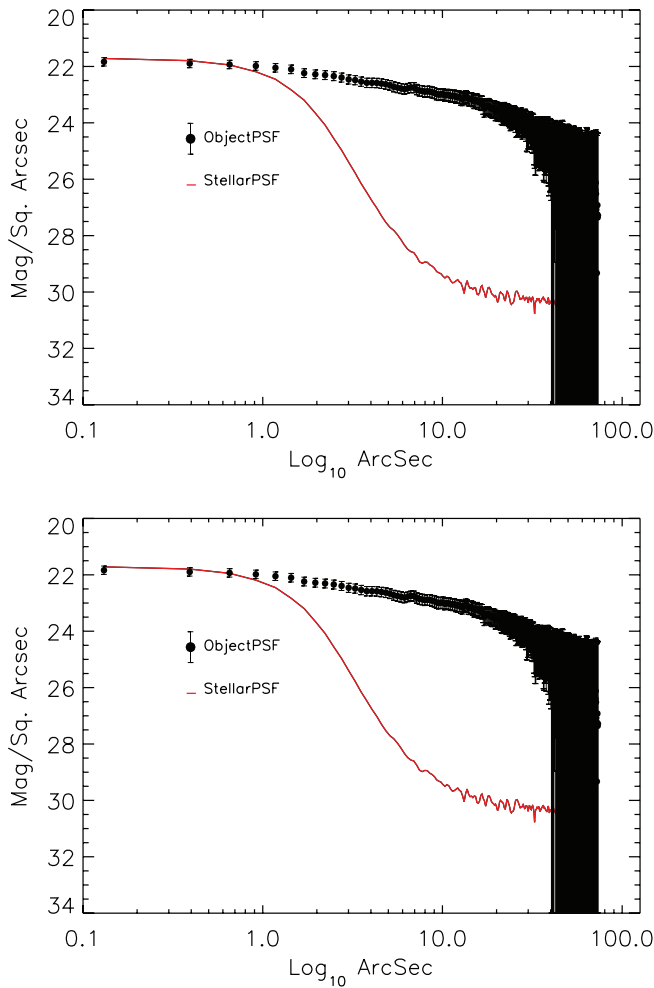


FIG. 4.—The *R*-band surface-brightness profile of the coma of Echeclus on the night of February 9 (top; TMO data) and on the night of the 2006 February 25 *Spitzer* observations (bottom). The two profiles appear very similar in shape and extent.

TABLE 5
ECHECLUS' *R*-BAND MAGNITUDES FROM 2006 FEBRUARY 04–27

Date	$m_R(5'')$	$H_R(\alpha, 1, 1)$
Feb 04/TMO	17.05 ± 0.03^a	5.98 ± 0.03
Feb 09/TMO	17.78 ± 0.02	6.73 ± 0.02
Feb 24/TMO	18.09 ± 0.02	7.08 ± 0.02
Feb 25/TMO, VATT, & Palomar ^b	18.10 ± 0.02	7.10 ± 0.02
Feb 26/Palomar	18.11 ± 0.02	7.11 ± 0.02
Feb 27/Palomar	18.11 ± 0.02	7.11 ± 0.02

^aThe color and magnitude uncertainties are from photon statistics.

^bPhotometry of Palomar and TMO agreed within 0.02 mag for the night of February 25.

havior, over week-long time scales, in combination with the hundredfold increase of the observed brightening compared to earlier observations (Bauer et al. 2003a; Rousselot et al. 2005), indicates a large degree of mass loss or a remarkably slow ejection velocity. Choi & Weissman (2006) have reported variations of coma features seen in Palomar observations that suggest a dust ejection velocity on the order of 200 m s^{-1} , ruling out the latter case.

3.2 *Spitzer* MIPS data

The 24 and $70 \mu\text{m}$ *Spitzer* MIPS data (Figs. 3 & 5) were reduced by two methods: the standard pipeline reduction (hereafter SPR; Engelbracht et al. 2007; Gordon et al. 2007), and the methods described by Stansberry et al. (2007, 2006; hereafter S07R). Our surface-brightness profiles were produced using the SPR mosaic images, and our photometry was conducted using the S07R images. The MIPS photometry results are listed in Table 6. The sky background was sampled at multiple points over a large fraction of the image to an uncertainty of ≤ 0.001 counts. The largest listed sampling apertures constitute $\geq 99\%$ of the total signal based upon the SBPs and the fact that apertures $\sim 2/3$ rds their size contained $< 2\%$ fewer counts. The S07R images provided data with noticeably less

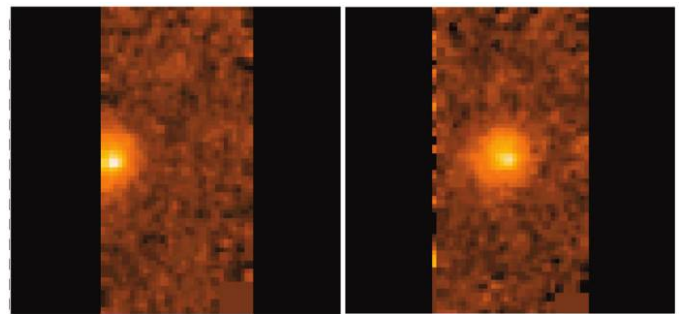


FIG. 5.—February 24 and 25 2006 $70 \mu\text{m}$ MIPS observations. The angular size of the *Spitzer* PSF at this wavelength is $\sim 18''$, and so the Centaur nucleus is not separately resolved from the coma's peak brightness. As with the other images in this paper, North is up, and East is to the left.

TABLE 6
 SPITZER PHOTOMETRY SUMMARY

<i>Spitzer</i> data set	Total Flux (mJy)	Flux, 60" Aperture	Flux, 30" Aperture	T_c [K] ^a 30"/60"	Derived $p_{v,\alpha}$ ^a 30"/60"	Comments
06 Feb 24-25, 24 μm	617 \pm 5	525 \pm 2	256 \pm 1	94.6 / 99.8	0.055/0.073	Total for 120" ap
06 Feb 25, 70 μm	201 \pm 3	199 \pm 2	126 \pm 2		0.35/0.54	Total for 80" ap
04 Jan 25 Cruikshank/Rieke		5 \pm 0.2		94	0.038 \pm 0.018	No coma, $R = 14.1$, $\Delta = 13.7$ (AU)
GTO, 24 μm						
04 Jan 25 Cruikshank/Rieke		16 \pm 4.0				No coma, "
GTO, 70 μm						

^a T_c Values for the 2006 February data are blackbody temperatures, and the listed albedo ($p_{v,\alpha}$) values are based upon T_c . The T_c (subsolar point) and $p_{v,\alpha}$ values for the 2004 January data are from Stansberry et al. (2007), where an STM model was used.

background noise, but the SPR images provided more point-source comparisons from the archive, necessary for the generation and interpretation of SBP analyses. Point-source comparisons were made from archival images of Chariklo and 2000 EC₉₈, i.e., Echeclus images without coma taken before the outburst (Cruikshank 2005; Stansberry et al. 2007). Both point sources compared well and provided low-noise SBPs out to sky background variations (Figs. 6 and 7).

The combination of visual and IR photometry allows for immediate derivation of an average coma-grain albedo and color temperature. However, the meaning of these values is broadly based on certain assumptions, most significantly that the particles viewed in the different IR wavebands are the same populations, and that these populations also dominate the visual signal. If this were the case, the color temperature would agree with the expected temperature value of particles heated by solar radiation at roughly 13 AU, the distance of Echeclus at the time

of the 2006 February observations. Furthermore, the albedo values as derived from combinations of the visual signal with those of the 24 and 70 μm photometry should at least overlap. It is very likely, however, that we do not view the same populations at the visual, 24, and 70 μm wavelengths (Fulle et al. 2004, and Discussion section) and that the color temperature (T_c) is not, in fact, the physical temperature of the grains (Kolokolova et al. 2004). We found the color temperature, based upon our two IR bands signals using 60" and 30" apertures, to be 97 ± 4 K, in excess of the 65–77 K expected for a blackbody with albedo ranging between 0.02 and 0.15. Coma measurements of comets in the infrared have yielded average color temperature excesses on the order of 10%–15% of blackbody temperatures (cf. Lisse et al. 1998; Tokunaga et al. 1988), but our derived value here is on the order of 27%. Derivations of the associated albedos for this color temperature using blackbody models (Lebofsky & Spencer 1989) yield albedo values

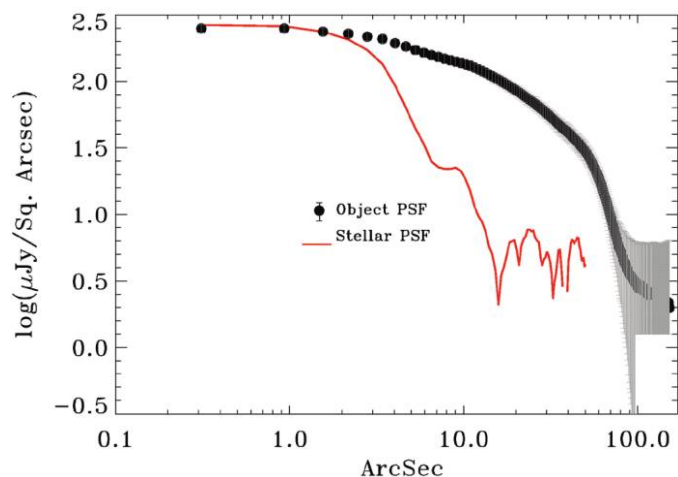


FIG. 6.—Surface brightness profile at 24 μm from the *Spitzer* 2006 February 25 observations. The stellar PSF was obtained from stars in the image. The behavior of the coma at this wavelength is similar to that in the ground-based R -band images, extending out to $\sim 90''$.

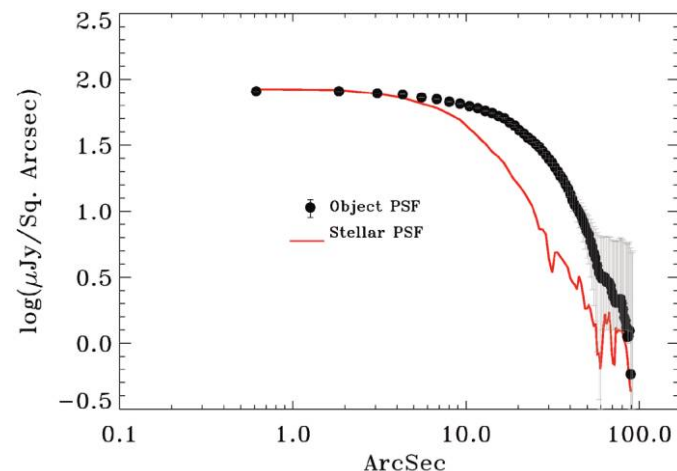


FIG. 7.—2006 February 25 70 μm MIPS surface-brightness profile from *Spitzer* data. The angular extent of the coma at this wavelength is $\sim 60''$, less than the visual R -band and 24 μm MIPS surface-brightness profiles. The stellar PSF was obtained from a combined mean of faint stars in the 70 μm image, and observations of other point sources from the SSC archive.

($p_{v,\alpha}$), uncorrected for phase, of 0.055–0.073 based on the fluxes observed at the 24 μm wavelength, which fall within a range only slightly higher than the surface albedo values observed prior to the 2006 outburst (Stansberry et al. 2007; see Table 6). However, for the albedo values derived from the 70 μm data, we find a considerably higher $p_{v,\alpha} \sim 0.4$. These temperature and albedo discrepancies may be attributable to our sampling of fluxes from different grain populations at our differing wavelength bands.

4. DISCUSSION

Our data reveal many interesting aspects of the most recently observed outburst of Echeclus. The *Spitzer* data in combination with the visual-band data place strong constraints on the dust-particle size distribution, and weak constraints on the Centaur's longevity with periodic outbursts of the nature observed during the 2005–2006 period. Discoveries of Choi et al. (2006a) and Weissman et al. (2006) yield particular details relevant to these analyses; primarily that the length of outburst was confined to the period within the 12 months spanning 2005 December–2006 December, and that the sky-plane velocity of coma features seen during Palomar imaging runs in the spring of 2006 indicate minimum dust ejection velocities (v_{ej}) on the order of 200 m s^{-1} .

The SBPs generated from the February 9 data (Fig. 4) show the extent of the coma to be $\sim 65''$, or a projected distance of 590,000 km. On February 25, both the visual (Fig. 4) and 24 μm (Fig. 6) images reveal a coma extent of 60"–70", or $\sim 580,000$ km, a comparable value to that of the February 9 data. In the 70 μm image from February 25, the coma extent was $\sim 60''$ or 530,000 km (Fig. 7). Hence, the scale of the coma seems fairly constant over several weeks and across a large range of wavelengths. Further evidence of a steady-state coma is given by linear fits to the SBPs. However, subsequent images during spring 2006 showed the coma continuing to grow and its peak moving relative to the Centaur (Weissman et al. 2006). As prescribed by Jewitt & Meech (1987) and Meech et al. (1997), we converted the SBPs to units of ln surface brightness ($\text{W m}^{-2} \text{Sr}^{-1}$) as a function of ln r (arcseconds), where r is the angular distance from the nucleus. Linear least-square fits were performed on the converted profiles for angular distances of 10" out to 60". $Af\rho$ values are nearly constant in this region, and small variations in the values may be attributable to low-level background fluctuations. We chose this range of angular distances for several practical reasons. First, deviations from the $1/r$ profile for distances less than 10" are likely due to the offset of the coma's central condensation from the nucleus. Second, beyond 10", the SBPs obtained from the visual data could be compared with the MIPS 24 and 70 μm SBPs without being affected by the poorer *Spitzer* resolution at the longer wavelengths. Finally, beyond 60", the signal-to-noise ratio dropped to less than 5 for most of the profiles, and close to 1 for the 70 μm SBP, as the signal approaches similar threshold levels

compared with sky background. The fits to the SBPs from the visual images taken on the nights of 2006 February 9 and February 25 yielded slopes of -1.07 ± 0.08 and -1.01 ± 0.01 , respectively, which were consistent with a canonical coma with surface brightness proportional to $1/r$. A slope of -1 is produced by an isotropic steady-state coma, while radiation pressure and phase angle effects may steepen the slope to values of -1.5 (Jewitt & Meech, 1987). Slopes steeper than -1.5 may be caused by non-steady-state emission or fading grains, while slopes shallower than -1 require a secondary source of grains with the coma, such as fragmenting grains (Meech et al. 1997). The slopes of the 24 and 70 μm MIPS images taken on 2006 February 25 yielded slopes of -1.3 ± 0.1 and -1.4 ± 0.1 , respectively, and so while somewhat steeper, could still be considered as consistent with a coma caused by steady-state outflow.

Over the span of the visual wavelengths observed, the coma is slightly redder than solar colors. Tables 3–5 list the results of the visual-band Bessel-filter B , V , R and I photometry, along with $Af\rho$ values (cf. A'Hearn et al. 1984). Color may be affected by both the intrinsic colors of the grains and by the particle size, which affects the ability of the particles to reflect light at wavelengths on the order of the particle size or larger. As implied by Kolokolova (2001), for cometary grains, the latter effect is the most dominant, so that the distribution of particle size may be weighted toward a scale of the order of 1 μm or larger for the case of Echeclus. Using the assumption of micron-sized grains, and constraints on the ejection velocity previously mentioned, estimates of the mass-ejection rates can be made from the visual data using the formula

$$Q_{\text{dust}} = Af\rho[(4/3\pi a^3 v_{ej} d_g)/(\pi a^2 p)] \quad (1)$$

where a is the mean grain size radius ($\sim 0.5 \mu\text{m}$), d_g is the grain density ($\sim 1 \text{ g cm}^{-3}$), and p is the average grain albedo, here ~ 0.04 and equal to that of Echeclus' nucleus (Stansberry et al. 2007).

This estimate, in fact, serves primarily as a lower bound, as particles may be larger than a micron, and the mass-ejection rates scale as a . Equation (1) itself is derived from the fact that the source of the coma must eject sufficient dust to fill the observed coma's extent in the time it takes the particles to cross out of the aperture used to derive a given $Af\rho$ value.

Similar arguments using scaling relations may be applied to derive estimates of instantaneous mass-ejection rates from the longer wavelength data. In the case of Echeclus, if we scale the surface area required to emit the observed flux of the coma relative to the signal of the nucleus, assuming the size and similar parameters derived from the 2004 bare-nucleus observations as in Stansberry et al. (2007; radius $R = 41.8 \pm 7.5$ km and albedo $p_v = 0.038 \pm 0.018$), we can derive an estimate of the quantity of dust in the coma. The mass-ejection rate can be further derived from a scaling of the ejection velocity.

A better estimate can be derived from the combination of the data sets across all wavelengths by subtracting out the contribution to the shorter wavelength signals from each of the longer wavelength's dust production.

Our scaling relations are aided by the fact that the 2006 *Spitzer* observations had very similar viewing geometry as in 2004, with a phase angle of 3.97° as compared with 3.7° in 2004, which would account for a difference of only $\sim 3\%$ in the signal, according to Rousselot et al. (2005). This offset is small compared to the $\sim 20\%$ formal uncertainty in the signal owing to the rotational light curve (Rousselot et al. 2005), the phase of which was unknown for either the 2006 or 2004 *Spitzer* data sets. Correcting for the heliocentric and observer distances along with the viewing phase, the 15.5 milli-Jansky (mJy) flux observed to be emanating from Echeclus' nucleus at a wavelength of $70 \mu\text{m}$ in 2004 should account for 21.8 mJy of flux, or 11% of the total signal listed in Table 6. Thus, the uncertainty owing to the unknown rotational phase should be $\sim 2\%$, leaving a flux value attributable to the coma of 180 ± 6 mJy. Similarly, the $24 \mu\text{m}$ flux value of the nucleus, observed to be 4.9 mJy in 2004, when rescaled to the 2006 *Spitzer* observing geometry accounts for 7.8 mJy of the total signal listed in Table 6, and the flux uncertainty from the unknown rotation phase is less than 1%, leaving a coma flux value of 610 ± 6 mJy, with the formal uncertainties folded in. The rescaled values are only for heliocentric distance and not rescaled for changes in temperature with heliocentric distance, which would introduce an additional change of $< 1\%$ in the total signal in either IR band.

Similar to the argument for visual-band reflection, a particle will be much less efficient at emitting radiation at wavelengths larger than its size (cf. Grün et al. 2001), and so we estimate the particle sizes viewed at 24 and $70 \mu\text{m}$ to be on the order of these observational wavelengths or larger (Fulle et al. 2004). What follows is a somewhat ad-hoc analysis. We have assumed that if the dominant particle size is less than the IR wavelengths, the grains become superheated, emitting at shorter wavelengths, in order to maintain equilibrium with the absorbed sunlight. However, this approach neglects the flux contribution at wavelengths longer than the particle size, which, though they would be nonzero, would also likely be relatively small. We can also estimate a maximum size particle capable of escaping the surface of the nucleus by using the model developed by Whipple (1951), modified by Jewitt & Matthews (1999) and summarized in Harmon et al. (2004). The maximum size, a_m , can be estimated within an order of magnitude by the equation

$$a_m = 9C_D v_g Z / 32\pi G R d_n d_g \quad (2)$$

where C_D is the dust drag coefficient, assumed here to be 2, as for a sphere, v_g is the gas ejection velocity, Z is the surface-gas mass flux, G the gravitational constant, R the radius of the

cometary nucleus (42 km; Stansberry et al. 2007), and d_n and d_g the densities of the nucleus and grains, respectively. An ejection velocity for the gas of $\sim 400 \text{ m s}^{-1}$ would be consistent with both the observations of Choi et al. (2006a) and CO as the source gas. A gas surface flux $Z \sim 5 \times 10^{-5} \text{ kg m}^{-2} \text{ s}^{-1}$ would be consistent with the flux of CO predicted by Meech & Svøren (2004) for Echeclus' heliocentric distance, so that, given densities of $\sim 1000 \text{ kg m}^{-3}$, a_m is approximately $700 \mu\text{m}$ for a nucleus the size of Echeclus. Caution should be used in taking the estimate provided by equation (2) too far beyond the accuracy of an order of magnitude, as the same values would yield a velocity scale factor, C_v , near unity, and v_t near 700 m s^{-1} for the terminal velocities of micron-sized grain particles (Harmon et al. 2004), which would be nearly a factor of 3 greater than those observed (Choi et al. 2006a), or nearly twice the ejection velocity of CO at Echeclus' distance. In any case, using the fact that the maximum grain size is only several hundred microns, but not likely cm scales, we can proceed at estimating the $70 \mu\text{m}$ contribution to the mass-loss rate.

We start by using the area of Echeclus' nucleus as a reference, and assume the emission properties as derived from the 2004 *Spitzer* images are similar to those of the grain particles in the coma during the 2006 observations. We estimate the effective area of the coma scaled by the relative fluxes to the total coma and the geometrically rescaled nucleus brightness values, as previously described, to derive an effective projected area for the particular wavelength observations, A_λ , of

$$A_\lambda = \pi R^2 \times (F_{\text{total},\lambda} - F_{\text{nuc},\lambda}) / F_{\text{nuc},\lambda} \quad (3)$$

where F_{total} is the total flux and F_{nuc} is the flux of the nucleus alone. The number of grains, n_g , can then be derived from the ratio of the projected area, A_λ , derived in equation(3) above to that of the area of a single dust grain, i.e.,

$$n_g = A_\lambda / \pi a^2 = (R/a)^2 \times (F_{\text{total}} - F_{\text{nuc}}) / F_{\text{nuc}} \quad (4)$$

The coma mass contribution of the grains of size a , $M_c(a)$, follows as a multiple of the number of grains, as derived from equation (4), and the mass per grain, $m_g = (4/3)\pi a^3 d_g$, where d_g is the grain density, assumed here, again, to be 1000 kg m^{-3} .

$$\begin{aligned} M_c(a) &= (4/3)\pi a^3 d_g n_g = A_\lambda (4/3) a d_g \\ &= (4/3)\pi a d_g R^2 \times (F_{\text{total}} - F_{\text{nuc}}) / F_{\text{nuc}}. \end{aligned} \quad (5)$$

Mass-loss rates can then be derived from the grain velocity, v_g , and projected size of the coma (or the portion being measured), R_c (similar to ρ in expressions of $A f \rho$), such that the crossing time for the material generated by the comet is $t_c = R_c / v_g$, and

$$Q_{\text{dust}} = M_c(a) / t_c = R_c [M_c(a) / v_g]. \quad (6)$$

TABLE 7
MASS-EJECTION ESTIMATES OF ECHECLUS

Particle radius	Q_{dust}^a (60" ap, kg s ⁻¹)	Q_{dust}^a (30" ap, kg s ⁻¹)	log(particle mass) (kg)	Total number of particles (60" ap)	Total number of particles (30" ap)
35 μm	1.7×10^3	2.0×10^3	-9.4236	1.2×10^{19}	7.1×10^{18}
12 μm	4.2×10^3	3.9×10^3	-10.8183	7.3×10^{20}	3.4×10^{20}
0.5 μm	3.3×10^2	3.3×10^2	-14.9589	1.2×10^{24}	5.4×10^{23}

^a As derived from the listed reference using the method outlined in Bauer et al. 2003b and in the text, assuming a grain density of $\rho \sim 1.0 \text{ g/cm}^3$. The Q_{dust} value is for a dust ejection velocity $v_{\text{ej}} \sim 200 \text{ m s}^{-1}$.

From Harmon et al. (2004), the grain velocity scales roughly as $a^{1/2}$. The estimates of Q_{dust} for 70 μm grains are listed in Table 7. We compare these values for aperture sizes with angular radii of 30" and for 60" as well, where the signal counts approach the noise levels in the SBPs for the 70 μm data. For the 24 μm dust mass production estimates, the technique was similar to that applied in equations (3)–(6) for the 70 μm data, except a term was subtracted from our estimate of total grain number $n_g(24 \mu\text{m})$ to compensate for the signal contribution from the 70 μm grains:

$$\begin{aligned} n_g(24 \mu\text{m}) &= [A_\lambda/\pi - n_g(70 \mu\text{m})(a = 35 \mu\text{m})^2]/(a \\ &= 12 \mu\text{m})^2. \end{aligned} \quad (7)$$

For the visual band, or $a = 0.5 \mu\text{m}$, the signal from the reflected light yielded the number of small grains from a similar argument:

$$\begin{aligned} n_g(0.5 \mu\text{m}) &= [(Af\rho \times \rho/p) - n_g(70 \mu\text{m})(a = 35 \mu\text{m})^2 \\ &- n_g(24 \mu\text{m})(a \\ &= 12 \mu\text{m})^2]/(a = 0.5 \mu\text{m})^2. \end{aligned} \quad (8)$$

Table 7 summarizes the mass-loss rates and model-dependant derivation parameters. The total mass loss is found here to still be largely in the form of small grains. A power-law fit to the log particle mass versus log grain size yields a slope, α_p , of -0.87 ± 0.1 (Fig. 8 and Table 8). The uncertainty in the slope parameter listed in Table 8 is derived from a linear regression fit to the particle log-masses and numbers in Table 7. The largest particles may have contained more mass, but reasonable estimates with upper bounds on the order of $\sim 3 \text{ mm}$ -sized grains would displace the derived number of particles by a factor of 7 fewer, and would further yield a fitted slope value within the listed uncertainties. When compared to the grain size distribution detected by the DFMI experiment on the *Stardust* spacecraft during the Wild 2 encounter (Green et al. 2004; $\alpha_p = -0.75 \pm 0.05$), our slope parameters agree within the errors to the particle size distribution found in 81P/Wild 2's inner coma.

The grain-size distribution does not agree with that of the Tempel 1 Deep Impact experiment. We have derived particle mass and number values at visual, NIR, and IR wavelengths

from the literature, applying our ad-hoc technique and previous equations. Schleicher et al. (2006) report visual-band $Af\rho$ values near 213 cm after impact, where Bauer et al. (2007) find 1.7 μm $Af\rho$ values near 724 cm following the impact, and Lisse et al. (2007) report IR flux values at 24 μm near 2000 mJy. Using equation (4) and scaling the measured nuclear fluxes of Lisse et al. (2005), we found values of $n_g \sim 2.8 \times 10^{17}$ for grain radii of 12 μm . For Tempel 1 $Af\rho$ values in the visual, applying equation (8), we find $n_g \sim 1 \times 10^{18}$ for particles of radius $a \sim 0.3 \mu\text{m}$, roughly half the observational wavelength, and $n_g \sim 7 \times 10^{16}$ for $a \sim 0.85 \mu\text{m}$ from the NIR data, so that the dust produced by the impact consists of considerably larger grains. Converting these values to dust masses, $M_c(a) \sim 4 \times 10^6 \text{ kg}$, on the order of the Jorda et al. (2007)

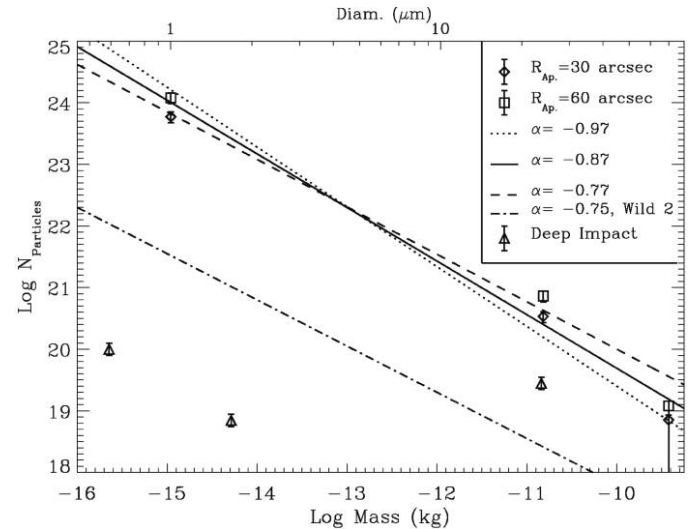


FIG. 8.—Estimated number of dust particles as a function of particle size and mass (both in \log_{10} units), based on the 2006 February 25 70 and 24 μm MIPS observations and the corresponding Palomar R -band observations, using a particle bulk density of 1.0 g/cm^3 . The derivation of the dust-grain numbers are as described in the text. The slope of the relation is independent of the assumptions of density and albedo, and the best-fit slope of -0.87 is similar to that derived from the cumulative fluence values of the DFMI on the *Stardust* spacecraft during the closest approach of the Wild 2 encounter (Green et al. 2004), shown for comparison. The particle size distribution is quite different for the Tempel 1 Deep Impact encounter, shown here as derived from the data of Schleicher et al. 2006, Bauer et al. 2007, and Lisse et al. 2007 after rescaling to 100 \times the values in the text for easier comparison on the plot.

TABLE 8
POWER-LAW FIT TO LOG-LOG PARTICLE MASS AND
NUMBER

Aperture	Y-intercept	Slope (power) ^a
30"	10.91 ± 1.02	-0.86 ± 0.08
60"	11.08 ± 1.21	-0.87 ± 0.10

^aMean-slope value is -0.87 ± 0.07 .

large-grain dust estimates. The “ad-hoc” technique, for our purposes of comparison, yields similar results for Tempel 1 as those derived from the more complete spectral data and extensive analysis. The implications for this comparison are that the outburst of Echeclus was likely induced by out-gassing activity similar to what is more typically seen as ambient comet behavior rather than generated by an impactor in the outer solar system.

If we assume a rate of $\sim 300 \text{ kg s}^{-1}$ and 6 months of such activity, we find a total mass loss of $4 \times 10^9 \text{ kg}$ per passage. Constraints on the physical lifetime of the comet are on the order of 10^9 years. This is a weak constraint considering the dynamical longevity of small bodies in this region of the solar system is $\sim 10^7$ years or less (cf. Horner et al. 2004).

5. CONCLUSIONS

Combined ground-based and *Spitzer* photometry reveals several characteristics of Echeclus’ activity:

1. The nucleus and coma were resolved in the visual and IR data sets, except at $70 \mu\text{m}$, where the instrument resolution was too poor to resolve the separation of $\sim 6''$.
2. Separation between the nucleus and coma brightness peaks was $\sim 6''$ (55000 km) on the plane of the sky.
3. The coma extended out $\sim 1'$ or greater in our visual and IR images, more than 500,000 km in projected distance from

Echeclus’ nucleus; this extent is approximately constant over timescales of weeks in 2006 February and over a large range of wavelengths.

4. The surface-brightness profiles suggest that the coma is generated by steady-state, isotropic, or nearly isotropic, outflow.

5. In both of the observed IR bands, the coma accounts for $>90\%$ of the observed signal.

6. Visual and IR dust production estimates indicate a dust-particle size distribution similar to that generated by typical cometary activity, as seen by the *Stardust* spacecraft’s encounter with 81P/Wild 2, for example. The particle size distribution is far less comparable to that generated by an impactor, as implied by the fluxes seen at varying wavelengths from the Deep Impact encounter with 9P/Tempel 1.

7. All estimates of mass loss exceed production estimates of other Centaurs and Jupiter family comets.

This research was funded in part by the General Observer program of *Spitzer*. The authors thank the SSC for their support. This work was performed in part at the Jet Propulsion Laboratory under contract with NASA, and was also supported to completion in part by the NASA Planetary Astronomy and Discovery Data Analysis Programs. Data were based in part on observations obtained at the Hale Telescope, Palomar Observatory, as part of a collaborative agreement between the California Institute of Technology, its divisions Caltech Optical Observatories and the Jet Propulsion Laboratory (operated for NASA), and Cornell University. Table Mountain Observatory is operated under JPL internal funds from the Science and Technology Management Council. This work was also partly based on observations with the VATT: the Alice P. Lennon Telescope and the Thomas J. Bannan Astrophysics Facility, and from observations obtained at the BOAO 1.8-m telescope. The authors thank the reviewer and editors for their valuable comments, which greatly enhanced the text.

REFERENCES

- A’Hearn, M. F., Dwek, E., & Tokunaga, A. T. 1984, *ApJ*, 282, 803
A’Hearn, M. F., Millis, R. L., Schleicher, D. G., Osip, D. J., & Birch, P. V. 1995, *Icarus*, 118, 223
Bauer, J. M., Buratti, B., Meech, K. J., Hicks, M. D., Fernandez, Y. R., & Bedient, J. 2004, *BAAS* 36, 1069
Bauer, J. M., Fernández, Y. R., & Meech, K. J. 2003b, *PASP*, 115, 981
Bauer, J. M., Meech, K. J., Fernández, Y. R., Pittichova, J., Hainaut, O. R., Boehnhardt, H., & Delsanti, A. C. 2003a, *Icarus*, 166, 195
Bauer, J. M., Weissman, P. R., Choi, Y.-J., Troy, M., Lisse, C. M., Dekany, R., Hanner, M. S., & Buratti, B. J. 2007, *Icarus*, 187, 296
Bessel, M. S. 1990, *PASP*, 102, 1181
Buzzi, L., Muler, G., Kidger, M., Heriquez Santana, J. A., Naves, R., Campas, M., Kugel, F., & Rinner, C. 2007, *IAU Circ.* 8886, 1
Choi, Y.-J., Cohen, M., Merk, R., & Prrialnik, D. 2002, *Icarus*, 160, 300
Choi, Y.-J., & Weissman, P. 2006, *BAAS*, 38, 551
Choi, Y.-J., Weissman, P., Chesley, S., Bauer, J., Stansberry, J., Tegler, S., Romanishin, W., & Consolmagno, G. 2006a, *CBET* 563, 1
Choi, Y.-J., Weissman, P. R., & Polishook, D. 2006b, *IAU Circ.* 8656, 2
Cruikshank, D. P. 2005, *Adv. Space Res.*, 36, 1070
Delsanti, A., Peixinho, N., Boehnhardt, H., Barucci, A., Merlin, F., Doressoundiram, A., & Davies, J. K. 2006, *AJ*, 131, 1851
Engelbracht, C. W., et al. 2007, *PASP*, 119, 994
Farnham, T. L. 2003, *BAAS*, 35, 971
Fulle, M. 1992, *Nature*, 359, 42
———. 1994, *A&A*, 282, 980
———. 2004, in *Comets II*, ed. M. C. Festou, et al. (Tucson: Univ. Arizona), 565
Gordon, K. D., et al. 2007, *PASP*, 119, 1019
Green, S. F., McDonnell, J. A. M., McBride, N., Colwell, M. T. S. H., Tuzzolino, A. J., Economou, T. E., Tsou, P., Clark, B. C., & Brownlee, D. E. 2004, *J. Geophys. Res.*, 109, E12S04
Grün, E., et al. 2001, *A&A*, 377, 1098
Harmon, J. K., Nolan, M. C., Ostro, S. J., & Campbell, D. B. 2004, in *Comets II*, ed. M. C. Festou, et al. (Tucson: Univ. Arizona), 265
Horner, J., Evans, N. W., & Bailey, M. E. 2004, *MNRAS*, 354, 798

- Jewitt, D. 2007, American Astronomical Society Meeting Abstracts, 210, #98.01
- Jewitt, D., & Matthews, H. 1999, *AJ*, 117, 1056
- Jewitt, D. C., & Meech, K. J. 1987, *ApJ*, 317, 992
- Jorda, L., et al. 2007, *Icarus*, 187, 208
- Kolokolova, L., Hanner, M. S., Lvasseur-Regourd, A.-Ch., & Gustafson, B. Å. S. 2004, in *Comets II*, ed. M.C. Festou, et al. (Tucson: Univ. Arizona), 577
- Kolokolova, L., Jockers, K., Gustafson, B. Å. S., & Lichtenberg, G. 2001, *J. Geophys. Res.*, 106, 10113
- Landolt, A. R. 1992, *AJ*, 104, 340
- Lebofsky, L. A., & Spencer, J. R. 1989, in *Asteroids II*, ed. R. P. Binzel, et al. (Tucson: Univ. of Arizona), 128
- Lisse, C. M., A'Hearn, M. F., Hauser, M. G., Kelsall, T., Lien, D. T., Moseley, S. H., Reach, W. T., & Silverberg, R. F. 1998, *AJ*, 496, 971
- Lisse, C. M., Kraemer, K. E., Nuth, J. A., Li, A., & Joswiak, D. 2007, *Icarus*, 187, 69
- Lisse, C. M., et al. 2005, *AJ*, 625, L139
- Lorin, O., & Rousselot, P. 2007, *MNRAS*, 376, 881
- Mazzotta Epifani, E., Palumbo, P., Capria, M. T., Cremonese, G., Fulle, M., & Colangeli, L. 2006, *A&A*, 460, 935
- Meech, K. J., Bauer, J. M., & Hainaut, O. R. 1997, *A&A*, 326, 1268
- Meech, K. J., & Belton, M. J. S. 1990, *AJ*, 100, 1323
- Meech, K. J., & Svøren, J. 2004, in *Comets II*, ed. M. C. Festou, et al. (Tucson: Univ. of Arizona), 317
- Prialnik, D., Brosch, N., & Ianovici, D. 1995, *MNRAS*, 276, 1148
- Rousselot, P., Petit, J.-M., Poulet, F., & Sergeev, A. 2005, *Icarus*, 176, 478
- Schleicher, D. G., Barnes, K. L., & Baugh, N. F. 2006, *AJ*, 131, 1130
- Schulz, R., & Stüwe, J. 2000, *BAAS*, 32, 1076
- Senay, M. C., & Jewitt, D. 1994, *Nature*, 371, 229
- Stansberry, J. A., Cruikshank, D. P., Grundy, W. G., Margot, J. L., Emery, J. P., Fernandez, Y. R., & Rieke, G. H. 2005, *BAAS*, 37, 737
- Stansberry, J., Grundy, W., Brown, M., Cruikshank, D., Spencer, J., Trilling, D., & Margot, J.-L. 2007, in *Kuiper Belt*, ed. M. A. Barucci, et al. (Tucson: Univ. Arizona), in press (S07R)
- Stansberry, J. A., Grundy, W. M., Margot, J. L., Cruikshank, D. P., Emery, J. P., Rieke, G. H., & Trilling, D. E. 2006, *ApJ*, 643, 556
- Stansberry, J. A., et al. 2004, *ApJS*, 154, 463
- Szabó, G. M., Kiss, L. L., Sárneczky, K., & Sziládi, K. 2002, *A&A*, 384, 702
- Tody, D. 1986, in *Instrumentation in Astronomy VI*, ed. D. L. Crawford, 733
- Tokunaga, A. T., Golisch, W. F., Griep, D. M., Kaminski, C. D., & Hanner, M. S. 1988, *AJ*, 96, 1971
- Weissman, P. R., Chesley, S. R., Choi, Y. J., Bauer, J. M., Tegler, S. C., Romanishin, W. J., Consolmagno, G., & Stansberry, J. A. 2006, *BAAS*, 38, 551
- Whipple, F. L. 1951, *ApJ*, 113, 464
- Womack, M., & Stern, S. A. 1995, *BAAS*, 27, 1143